REDUCTION OF TURBULENT SKIN FRICTION BY MICROBUBBLES

N. K. Madavan, S. Deutsch & C. L. Merkle

Technical Memorandum
File No. TM 83-23
9 March 1983
Contract No. N00014-81-K-0481

Copy No. 1

The Pennsylvania State University
Intercollege Research Programs and Facilities
APPLIED RESEARCH LABORATORY
Post Office Box 30
State College, PA 16801

UNCLASSIFIED

SECURITY CLASSIFICATION OF THIS PAGE *(When Data Entered)*

REPORT DOCUMENTATION PAGE		READ INSTRUCTIONS BEFORE COMPLETING FORM
1. REPORT NUMBER TM 83-23	2. GOVT ACCESSION NO.	3. RECIPIENT'S CATALOG NUMBER
4. TITLE *(and Subtitle)* REDUCTION OF TURBULENT SKIN FRICTION BY MICROBUBBLES		5. TYPE OF REPORT & PERIOD COVERED Technical Memorandum 6. PERFORMING ORG. REPORT NUMBER
7. AUTHOR(s) N. K. Madavan, S. Deutsch and C. L. Merkle		8. CONTRACT OR GRANT NUMBER(s) N00014-81-K-0481
9. PERFORMING ORGANIZATION NAME AND ADDRESS Applied Research Laboratory Post Office Box 30 State College, PA 16801		10. PROGRAM ELEMENT, PROJECT, TASK AREA & WORK UNIT NUMBERS
11. CONTROLLING OFFICE NAME AND ADDRESS Office of Naval Research, Code 474 800 North Quincy Street Arlington, VA 22217		12. REPORT DATE 9 March 1983 13. NUMBER OF PAGES 36
14. MONITORING AGENCY NAME & ADDRESS*(if different from Controlling Office)*		15. SECURITY CLASS. *(of this report)* Unclassified 15a. DECLASSIFICATION/DOWNGRADING SCHEDULE

16. DISTRIBUTION STATEMENT *(of this Report)*

Approved for public release. Distribution unlimited.
Per NAVSEA- March 31, 1983.

17. DISTRIBUTION STATEMENT *(of the abstract entered in Block 20, if different from Report)*

18. SUPPLEMENTARY NOTES

19. KEY WORDS *(Continue on reverse side if necessary and identify by block number)*

microbubble, reduction, turbulent, skin, friction

20 ABSTRACT *(Continue on reverse side if necessary and identify by block number)*

Measurements of the effect of microbubbles on a zero pressure gradient turbulent boundary layer generated on the test section wall of a water tunnel are described. Microbubbles were created by injecting air through a 0.5 μm sintered stainless steel plate immediately upstream of a floating element drag balance. At the downstream edge of the balance the length Reynolds number was as high as ten million. →

DD FORM 1 JAN 73 1473 EDITION OF 1 NOV 65 IS OBSOLETE

UNCLASSIFIED

(cont)

Integrated skin friction reduction of greater than 80% was observed. The drag balance results were confirmed by measurements with surface hot film probes. For the case in which buoyancy tended to keep the bubbles in the boundary layer, the skin friction data was shown to collapse when plotted against the ratio of air to water volume flow rate. The effects of buoyancy on skin friction reduction were also documented.

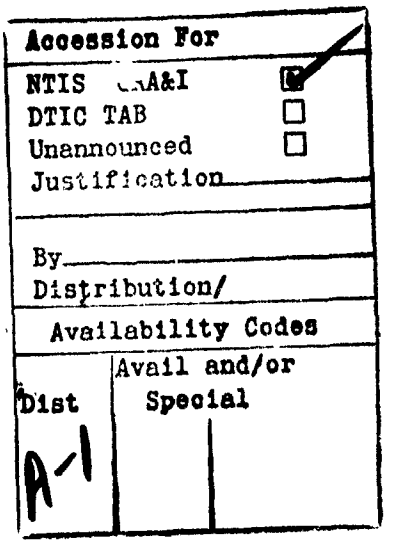

Subject: Reduction of Turbulent Skin Friction by Microbubbles

References: See Page 18

Abstract: Measurements of the effect of microbubbles on a zero pressure gradient turbulent boundary layer generated on the test section wall of a water tunnel are described. Microbubbles were created by injecting air through a 0.5 μm sintered stainless steel plate immediately upstream of a floating element drag balance. At the downstream edge of the balance the length Reynolds number was as high as ten million. Integrated skin friction reduction of greater than 80% was observed. The drag balance results were confirmed by measurements with surface hot film probes. For the case in which buoyancy tended to keep the bubbles in the boundary layer, the skin friction data was shown to collapse when plotted against the ratio of air to water volume flow rate. The effects of buoyancy on skin friction reduction were also documented.

INTRODUCTION

Some initial results of an experimental program directed towards assessing the effects of very small gas bubbles (microbubbles) on a liquid turbulent boundary layer are described. For the most part, the gas of interest is air and the liquid is water. The experiments are stimulated by a desire to reduce the skin friction in a turbulent boundary layer. Although the results obtained thus far are encouraging, it is too soon to speculate if this technique is to have engineering benefits.

Microbubble drag reduction studies are perhaps an outgrowth of the age-old idea of placing a layer of air between a ship and its water boundary layer to reduce the skin friction. This idea was patented in the 1800's (1), although its practicality seems highly improbable, if, for no other reason than the instability of the air-liquid interface so generated. The use of very small bubbles eliminates this air-film instability while retaining many of the benefits of the original concept.

The first experimental work on the microbubble problem was reported by McCormick and Bhattacharyya (2) in 1973. They used a copper wire wound around a towed body of revolution to produce hydrogen bubbles by electrolysis. Their measurements demonstrated that the total drag on the body was reduced when the hydrogen bubbles were present, particularly at the lower Reynolds numbers. The decrease in effectiveness of the bubbles at the higher Reynolds numbers was apparently attributable to limitations on the mass generation rate of hydrogen. Their results also demonstrated that the amount of drag reduction increased monotonically with electrical current and, hence with the hydrogen flow rate. Unfortunately, the presence of pressure gradients and boundary layer transition made it difficult to separate the effects of skin friction and form drag or to study the detailed mechanisms whereby the drag reduction

was realized. In addition, the results were limited to Reynolds numbers between 0.3 and 1.8 million. Nevertheless, the overall implications of these results are significant in that the total drag on the body was decreased by the bubbles.

The effects of microbubbles on a turbulent boundary layer have also been studied by a group of Soviet scientists (3-6). Instead of using electrolysis to generate the bubbles, they forced air thrcugh a porous surface with pore sizes ranging from 1 to 50 μm. Their experiments were conducted using a simple flat plate geometry with all measurements being made downstream of the porous section. The measurements included the local skin friction, the transverse variation of the bubble concentration and some portions of the velocity profiles. The results indicated that the local skin friction could be reduced to nearly 10% of its undisturbed value by microbubble injection. The maximum skin friction reduction was observed to occur near the porous section while further downstream the boundary layer gradually relaxed back toward its undisturbed condition. The parameters that control the characteristic length which describes this relaxation were not determined, but are probably attributable to the migration of the microbubbles outside the boundary layer. Such migration could occur through the effects of diffusion, buoyancy, or interaction with the local mean velocity gradient. It appears that the Soviet experiments were performed with the boundary layer above the porous surface so that the effect of buoyancy was to remove the bubbles from the boundary layer.

In contrast to the general result that microbubbles decrease the skin friction, it was noted that at the lowest tunnel velocities a small concentration of bubbles caused the skin friction to increase slightly (4). Since the characteristics of the undisturbed boundary layer were not reported, a conclusive explanation for this observation cannot be given, but it appears

likely that the increase occurred because the bubbles tripped a laminar boundary layer.

The bubble concentration measurements reported in Refs. (3-6) showed a peak at a y/δ location of about 0.1. The magnitude of the volumetric concentration at this peak was as high as 80%. Near the wall, and in the free stream, the bubble concentration was characterized by a fall-off to zero. By taking advantage of the absence of bubbles near the wall, the Soviet researchers made some LDA measurements of the near-wall velocity profiles. They found that the LDA signal became too weak for use at bubble concentrations exceeding 3%, so they were only able to measure out to $U/U_\infty \approx 0.4 - 0.6$ depending on the shape of the profile. These near-wall velocity measurements showed clear evidence of a reduction in velocity gradient at the wall as the airflow rate was increased. Further, skin friction estimates based on these slopes were in reasonable agreement with the more direct skin friction measurements alluded to earlier which were obtained with surface-mounted hot films (3), and small, flush-mounted floating element balances (4,5).

The bubble sizes which are generated as the air flows through the porous material represent an additional important parameter of the microbubble boundary layer. References (3-6) reported bubble diameters ranging from submicron size to as high as 50 μm. These estimates were based upon injection into quiescent water, and on a break-up criterion suggested by Hinata and Ohki (7) which is based on the Weber number of the bubbles. Silberman (8) and Hughes et al (9) have reported measurements of bubble injection from a single orifice into a flowing liquid and have noted that the diameter is independent of hole size and depends only on the ratio of the flow rates of the two streams. No conclusive data concerning the variation of bubble sizes from a porous material into a flowing liquid appear to be available.

The results described in the present paper are directed towards investigating the basic physics of a turbulent boundary layer saturated with microbubbles. The primary data reported herein are measurements of the integrated skin friction downstream of a porous air injection section as a function of the air flow rate and the free-stream velocity. Data are presented for three different plate orientations with respect to gravity. Auxiliary measurements include LDA and hot film surveys of the undisturbed boundary layer to document the characteristics of the boundary layer into which the bubbles are injected, plus a few mean flow measurements in the outer part of the boundary layer in the presence of bubbles. Some local skin friction measurements at a single point on the surface are also reported.

EXPERIMENTAL FACILITY

The experiments were conducted at The Pennsylvania State University, in a water tunnel at the Applied Research Laboratory. The rectangular test section had dimensions of 508 mm by 114 mm by 762 mm long. Both tunnel velocity and pressure are continuously controllable, with a maximum test section velocity of about 25 m/s and tunnel pressures ranging between 0.2 and 4 atm. The test section can be rotated at 90° intervals to allow buoyancy effects to be studied. In addition, a 0.2 cu.m/s bypass (roughly 15% of the tunnel volume flow rate at maximum speed) can be employed to keep the tunnel relatively air free. Tunnel turbulence control is through a 152.4 mm section of honeycomb with a 25.4 mm core size and a 9:1 contraction section. The free-stream turbulence intensity was measured to be 0.3-0.5% over the velocity range of interest.

The flat plate on which the measurements were performed was mounted in one wall of the rectangular test section in a 279 mm wide by 533 mm long opening intended for a window. Centered spanwise on the test plate was a

102 mm by 178 mm porous sintered stainless-steel section for gas injection, followed by a 102 mm by 254 mm force balance, as shown in Fig. 1. The sintered stainless-steel plate is manufactured by Mott Metallurgical Corp. for use as a filter. The filter type chosen will trap particles of diameter 0.5 μm and larger. This corresponds to a nominal pore size of about 5.0 μm. An appropriate roughness height for the sintered porous plate is 1.6 μm as estimated by comparison with surface roughness gauges.

INSTRUMENTATION

The floating-element force balance which was used for the skin friction measurements employed a strain-gaged tension/compression member to infer integrated skin friction on the surface. Clearances around the balance, at no flow, were nominally 0.038 mm at the leading edge, 0.25 mm at the trailing edge and 0.10 mm on either side. Sealing around the force balance was avoided by filling the cavity underneath the balance with water, as shown on Fig. 1. Dry calibration showed excellent linearity to an applied force of ten newtons (corresponding to the turbulent shear force produced at a free stream velocity of 18 m/s). Calibration against water velocity in the absence of microbubbles, was done often, and the force balance was found to be very stable. Throughout the tests, the force measurements with and without microbubbles were very repeatable.

The test section velocity was determined from a Validyne Model DP15 pressure transducer which measured the pressure drop across the tunnel contraction section. Calibration of the transducer was made before and after the experiments. Simple single-point checks were also employed during the runs.

Injected gas flow rates were measured using a Flow Technology FT12 M18-GB turbine flow meter and a second Validyne transducer. For some of the early experiments, a F&P Co. Precision Ball Flowrater rotameter was used to determine the gas volume flow rate. Factory calibration of the turbine flow meter was assumed valid. Comparison of the data taken using the rotameter with that taken using the turbine meter indicated that this assumption was reasonable.

Tunnel velocity, integrated skin friction, gas pressure and gas volume flow rate were visually monitored on integrating digital voltmeters and simultaneously recorded on two Nicolet Model 206 digital oscilloscopes. The digital readout of the tunnel velocity was used manually to maintain constant tunnel speed during the run. The oscilloscopes performed an analog-digital conversion and stored the data on floppy disks. Each channel of the oscilloscope has a storage capacity of 2048 points. Data was normally taken at the rate of five points per second, so that run times were approximately seven minutes in duration. During a run, the skin friction was first measured with no airflow. The airflow was then increased to its maximum allowable value while taking data at the five-point-per-second rate. After reaching maximum flow rate, data taking was continued while the flow was again reduced to zero. Inspection of the data indicated excellent agreement between the data taken while the air flow was increasing and decreasing and the skin friction showed excellent repeatability in returning to its original zero-airflow value after the flow was turned off. Data reduction and analysis was performed on the Penn State IBM 3033 system, and those data points for which the velocity varied by more than ± 1% from the mean were excluded.

Local skin friction was also measured at a single location on the plate as shown in Fig. 1. A TSI Model 1471-W surface mounted hot-film probe and a DISA 55M01 anemometer were used for the measurements. (These flush-mounted

hot film data were recorded on the Nicolet and computer-linearized whereas the conical probe data described later were linearized by means of an analog device and recorded manually). Time averaged values of the local shear stress were deduced from Nicolet records which were recorded at the rate of 20,000 points per second allowing a record length of about 0.1 s. Repeatability checks at constant tunnel conditions indicated that this record length was sufficient to resolve the mean skin friction. In addition to these short time records, some long time records (approximately 5 minutes) were recorded on a Spectral Dynamics Model 350 Digital Signal Processor and used to obtain spectral information on the local shear stress. The calibration of the hot film was accomplished by plotting the output voltage as a function of free-stream velocity (in the absence of bubbles) versus the local skin friction as determined from classical turbulent boundary layer correlations. In this process, the mean skin friction was used as a check.

In addition to the skin friction measurements, the velocity and turbulence intensity profiles of the boundary layer into which the micro-bubbles were injected were surveyed by means of both a conical hot film probe and a laser doppler anemometer (LDA). Both these surveys were limited in proximity to the wall; the hot film was limited by the size of the probe, while the LDA was limited by reflection from the wall. (The LDA measurements could only be obtained by entering the boundary layer from the free-stream side with the beam directed normal to the wall so that reflection from the wall limited the deepest penetration into the boundary layer.) Both the LDA and hot-film techniques reached approximately the location where $U/U_\infty \approx 0.6$. In addition to surveying the boundary layer without air, both techniques were also tried with microbubbles present.

The hot film measurements were made with a traverse mechanism which allowed positioning at 8.5 μm intervals. An estimate of the uncertainty in the vertical placement of the probe is 42.5 μm. Initial probe position was determined by placing the probe on the test plate while the tunnel was in operation.

The LDA measurements wer taken with an 8-watt Argon ion laser and a TSI Model 1980 counter processor. Backscatter optics were employed with a 3.75 X beam expander and a 480 mm transmitting lens, providing an ellipsoidal sampling volume of 80 μm in the vertical and streamwise directions and 580 μm in the cross-flow direction. Positioning in the boundary layer was accomplished using an NRC Model 280 precision jack and monitored by a dial gauge with 25.4 μm gradations. LDA data acquisition and reduction was performed on a minicomputer interfaced to the LDA counter processor. Output was presented on a video screen in the form of a histogram for each measurement point in the boundary layer. The mean velocity, turbulence intensity, and percent of samples retained in the calculations (a rough indication of the signal-to-noise ratio) were also printed on the screen. For the measurements in the outer part of the boundary layer, nearly 100% of the samples were used. At the location closest to the wall, this percentage dropped to about 80% when microbubbles were present. No corrections to the turbulence intensity were employed. The tunnel has been frequently seeded with 1.5 μm silicon carbide particles and these are the most probable source for laser scattering.

Since neither the hot film nor LDA velocity profiles were recorded on the Nicolet oscilloscopes, manual control of the mean velocity, particularly for the measurements with bubble injection, should be taken to imply control to ± 5%.

RESULTS AND DISCUSSION

Integrated Skin Friction Measurements

Integrated skin friction measurements both with and without microbubbles were obtained for tunnel velocities ranging between 4.2 and 17.4 m/s. This corresponds to length Reynolds numbers between 2.2 and 10.6 million at the downstream edge of the metric section. The corresponding Reynolds numbers at the upstream end of the porous section are 0.7 and 3.0 million. These Reynolds numbers are based on a fictitious boundary layer origin 180 mm upstream of the porous section. This fictitious origin was obtained from the boundary layer thickness measurements described later. The maximum Reynolds number in the present experiments is nearly a factor of two higher than that used in Refs. (3-6). The measurements included tests with the plate on the top of the tunnel, on the bottom, and on the side. In addition, measurements were also conducted using helium instead of air as the test gas.

Measurements of the skin friction in the absence of microbubbles are given on Fig. 2 as a function of Reynolds number. The C_f-Re data exhibit a slope of - 0.21 with the C_f values ranging between 0.005 and 0.006. For comparison, results for a classical, smooth wall, turbulent boundary layer (10) are also included on Fig. 2.

The airflow rates used to generate the microbubbles ranged as high as 5×10^{-3} m^3/s. On the basis of airflow per unit width of porous surface, these values are some five times larger than the maximum rates used in Refs. (3-6).

As indicated previously, a total of 2048 data points were taken in each run at a rate of five points per second. During this time, the tunnel velocity was held constant while the airflow was slowly varied from zero to the maximum and back to zero again. Two independent methods were used for evaluating the data comprising each constant velocity run. In the simplest

procedure 50 data points were sampled at random from the complete set. This method gave a good representation of the skin-friction/air-flow behavior, but it gave no statistical information as to the expected data scatter. To remedy this, the second method was used. In this method the data were grouped into specified airflow intervals or bins and the data in each bin was averaged to find the mean data line. Bins were spaced evenly in 0.5×10^{-3} m^3/s airflow intervals with widths of 0.025×10^{-3} m^3/s. Confidence levels in each bin were determined by the Student T of F test. Bin populations ranged between 10 and 100 samples. The average curve as determined by this latter method was in excellent agreement with that obtained by the former.

The effect of microbubbles on the integrated skin friction for the case where the plate is on the top of the tunnel is given in Figs. 3 and 4. In this configuration, buoyancy tends to retain the bubbles in the boundary layer. Figure 3 shows that for all velocities the skin friction begins decreasing as soon as the airflow is turned on and continues to do so until, at the higher airflow rates, it approaches a constant minimum value. At the lower tunnel velocities the skin friction decrease is more pronounced because a given amount of airflow corresponds to a larger volumetric concentration of air in the boundary layer than at the higher speeds. The maximum observed skin friction reduction was in excess of 80% (see Fig. 3) and occurred at a tunnel velocity of 4.2 m/s and an airflow of 4.0×10^{-3} m^3/s.

In Fig. 4, the C_f/C_{f_o} ratio for data taken with the plate on top is plotted against the nondimensional variable $O/U_\infty A$, where O is the gas flow rate, U_∞ is the tunnel speed, and A is a reference area. For the present figure, this area has been taken as the wetted surface area of the porous plate. Note that this choice implies that $O/U_\infty A$ is the ratio of the effective velocity of the incoming air to the tunnel velocity. Perhaps a better area would be the cross-sectional area of the boundary layer (the displacement

thickness times the width) in which case the nondimensional ratio would compare the volumetric flux of air to the volumetric flux of water in the boundary layer. Note that the use of this parameter causes the data to collapse to a single line indicating that with the plate on top this parameter gives a unique skin friction correlation for all tunnel speeds.

The results plotted in Fig. 5 represent one set of data taken with helium as the injected gas, as well as one set of data taken with airflow through only the downstream half of the porous section. The helium and half-porous section data also collapse quite reasonably when presented in terms of $Q/U_\infty A$. The collapse of the helium data indicates that it is the volumetric concentration of the microbubbles and not their mass concentration which is the relevant parameter. Thus, the momentum of the incoming gas does not appear to be a parameter. The collapse of the half-plate data (note that the same area was used in $Q/U_\infty A$ for the half-plate as for the full-plate) indicates that the distance over which the bubbles are injected is not particularly important, but again that it is the volumetric flow rate.

The skin friction for the two other plate orientations is given on Figs. 6 and 7 along with a comparison to the data for the plate on top. The comparison at the lower speed (9.3 and 9.6 m/s) clearly shows that buoyancy effects are present at this speed. Direct comparison at higher velocities is not available, but extrapolation of the plate on top data suggests that the effects of buoyancy are smaller at the 14 m/s speed. In particular, the results show that at the lower speeds the skin friction reduction is considerably less than with the plate on top.

The effects of buoyancy appear to be somewhat stronger when the plate is vertical than when it is on the bottom of the boundary layer. An interesting phenomenon was observed at low speeds (< 2.5 m/s) with the plate in the vertical position. It was noted that the bubbles would remain spread out and

close to the surface with seemingly little buoyancy effect for a while. Then, suddenly the entire gas "film" would roll up into a convoluted surface which was highly buoyant and would be swept up and away from the force balance. When this roll-up occurred, the skin friction would immediately return to its gas-off value. These rolled-up and dispersed bubble configurations appeared to be bi-stable and one configuration would instantaneously change to the other for no apparent reason. This phenomenon was not observed at tunnel speeds above 2.5 m/s.

Local Skin Friction Measurements

The local skin-friction, as measured with the flush-mounted hot-film probes at the position shown in Fig. 1, is presented in Fig. 8. These data were taken with the plate on the bottom. The local skin-friction reduction for a given airflow exceeds that obtained with the integrated measurements as can be seen by comparison with Fig. 6. This is to be expected, because the hot-film probe is relatively close to the porous injection plate so that the microbubbles have had little time to escape from the boundary layer. For these data, microbubble impingement on the hot-film probe was never observed whereas for the conical probe in the boundary layer, bubble impingement was detected fairly often. This is in agreement with earlier observations (5) that a bubble-free region exists close to the wall when the plate is on the bottom.

It could also be observed from the oscilloscope trace of the flush-mounted hot-film probe that the microbubbles decreased the amount of high-frequency information substantially as compared to the no airflow case. This loss of high frequency information in the presence of microbubbles was confirmed quantitatively from spectra taken on the Spectral Dynamics frequency analyzer. The loss of high frequency scales suggests a decrease in the

turbulent Reynolds number such as would be generated by the increase in viscosity and decrease in density expected from the bubbles.

Characterization of the Boundary Layer with and without Microbubbles

The static pressure distribution in the tunnel was measured at ten locations along the length of the test section using flush-mounted surface taps on the tunnel wall opposite the test plate. The measurements, which are shown on Fig. 9, indicate that the pressure varied by less than ± 0.7% of the dynamic head over the length of the test section. With the maximum flow rate of bubbles, the pressure at any given tap changed by less than ± 0.25%.

In order to document the undisturbed boundary layer into which the bubbles were generated, mean velocity profiles and turbulence intensities were measured at several stations. Conical hot film measurements were made at a free-stream velocity mean of 4.6 m/s; LDA data were taken at 7.6 m/s. The mean profiles are shown in outer variables on Fig. 10. The boundary layer thickness used for nondimensionalizing these data are based upon the location at which the velocity reaches 0.99 of the free stream. (This variation is presented in the inset on Fig. 10.) For comparison, the one-seventh power law profile is also shown. Turbulence intensities corresponding to the mean profile are given on Fig. 11.

A comparison of LDA data taken with and without microbubbles is given in Fig. 12. These data, which were taken at a free-stream velocity of 7.5 m/s and an airflow rate of 0.5×10^{-3} m^3/s, indicated a slight broadening in the velocity histogram when bubbles were present because of the introduction of more low-speed data points. (These could have been samples scattered from large bubbles which were lagging the local mean velocity.) As can be seen, the presence of the microbubbles certainly causes no dramatic realignment of the characteristics of the outer boundary layer. Instead the velocities

appear to be somewhat lower than they were in the absence of bubbles (as would be expected for a weaker gradient at the surface) but otherwise are nearly unchanged. Qualitative data taken with the conical hot film probe also showed the same trends.

The corresponding turbulence intensities for the boundary layer with microbubbles are given in Fig. 12. Again, these data show no major changes in the character of the outer boundary layer ($y^+ > 100$) in the presence of the microbubbles.

A POTENTIAL MECHANISM FOR THE EFFECTS OF MICROBUBBLES

The specific reduction mechanism remains a matter of conjecture, and must remain so until detailed velocity profiles an gas concentration profiles in the near wall region of the boundary layer can be made. Still, with the experimental data presented here it could be argued that the drag reduction mechanism is similar to that acting in polymer solutions.

Polymer drag reduction has been described by Lumley (11,12). Briefly, outside the viscous sublayer of a high Reynolds number turbulent boundary layer, the rotation and strain rate fields are uncorrelated. Polymer molecules found these will stretch resulting in increased solution viscosity. This additional viscosity (or decreased Reynolds number) will increase the size of the smallest eddies capable of surviving. Just outside the sublayer (the buffer region) where Reynolds stress-producing eddies are roughly the size of the Kolmogorov eddies, the turbulence is dissipated. The sublayer thickness increases and the skin friction is reduced. The same case can be made for certain types of particles in the flow (11).

In the case of microbubble injection, the viscosity in the sublayer is unaffected because of the absence of bubbles there. Outside this region the bubbles cause both an increase in the absolute viscosity through an

Einstein-type relation and a decrease in the solution density. Again, this results in a thicker sublayer.

CONCLUSIONS

The effects of injecting a high concentration of microbubbles into a turbulent boundary layer have been studied experimentally. The microbubbles were generated by injecting air (or helium) through a sintered stainless steel porous plate whose nominal pore size is 5.0 μm. Instrumentation included a floating-element force balance 254 mm in length which was situated immediately downstream of the porous section and a flush-mounted hot film probe 51 mm downstream of the injection section. The characteristics of the boundary layer into which the bubbles were injected were surveyed with a conical hot film probe and a LDA. The results show that the integrated skin friction was reduced for all air flow rates and tunnel velocities. Maximum reductions of more than 80% were observed. With the plate on the top of the tunnel, the ratio of the skin friction in the presence of microbubbles to that without microbubbles could be collapsed to a single curve by nondimensionalizing the volumetric airflow rate by the water velocity and an appropriate area. This same collapse of data could not be obtained with the plate on the bottom of the tunnel because in this orientation the effects of gravity enter as an additional parameter. With the plate on the bottom, the data at the lower tunnel speeds indicated that the reduction in skin friction was substantially less than was observed with the plate on the top. At the higher speeds, the observed effects of gravity were smaller. This indicates that the present tests nearly spanned the domain in which buoyancy effects are and are not significant for the present force balance length, tunnel speeds and range of bubble sizes.

Local skin friction measurements with the flush-mounted hot-film probe were in qualitative agreement with these integrated skin friction data. Spectra from the hot film probe showed that the presence of microbubbles caused a shift in the turbulence peak toward lower frequencies suggesting a reduction in the turbulent Reynolds number. The oscilloscope trace of the hot film showed no evidence of gas bubble impingement, supporting the notion of a bubble-free layer near the wall.

Velocity and turbulence intensity profiles in the outer region of the boundary layer showed no dramatically different character when microbubbles were present as compared to when they were absent. This lends credence to the concept of a boundary layer modified by the presence of microbubbles as opposed to a complete restructuring of the flowfield when microbubbles are introduced.

Finally, we note that overall the present results are in qualitative agreement with earlier experiments (3-6). Several parameters have been varied over wider ranges, and effects of gravity have been documented for the first time.

ACKNOWLEDGMENT

This work was sponsored by the Office of Naval Research under Contract Number N00014-81-K-0481.

REFERENCES

1. P. R. Grewe and W. J. Eddington, Quart. Trans. Roy. Inst. Nav. Arch., p. 102 (1960).

2. M. E. McCormick and R. Bhattacharyya, Nav. Eng. J. 85, p. 11 (1973).

3. Yu. N. Dubnischev, E. R. Evseev, V. S. Sobolev and E. N. Utkin, J. Appl. Mech. Tech. Phys. 16, No. 1, p. 114 (1975). Translated from Zhur. Prikl. Mekh. Tekh. Fiz., No. 1, p. 147 (1975).

4. G. S. Migirenko and A. R. Evseev, Problems of Thermophysics and Physical Hydrodynamics (in Russian), (Novosibirsk, Nauka, 1974).

5. V. S. Bogdevich and A. G. Malyaga, in Investigations of Boundary Layer Control (in Russian), edited by S. S. Kutateladze and G. S. Migirenko (Thermophysics Institute Publishing House, 1976), p. 62.

6. V. G. Bogdevich and A. R. Evseev, in Investigation of Boundary Layer Control (in Russian), edited by S. S. Kutateladze and G. S. Migirenko (Thermophysics Institute Publishing House, 1976), p. 49.

7. S. Hinata and M. Ohki, Bull. Jap. Soc. Mech. Eng. 14, p. 951 (1971).

8. E. Silberman, presented at the Fifth Midwestern Conference on Fluid Mechanics, University of Michigan (1957).

9. N. H. Hughes, M. M. Reischman and J. M. Holzmann, presented at the Sixth Biennial Symposium on Turbulence, University of Missouri, (1979).

10. H. Schlichting, Boundary Layer Theory (McGraw-Hill, New York, 1979), p. 638.

11. J. L. Lumley, Phys. Fluids 20, Pt. II, S64 (1977).

12. J. L. Lumley, J. Polymer Sci., Macromol. Rev. 7, p. 263 (1973).

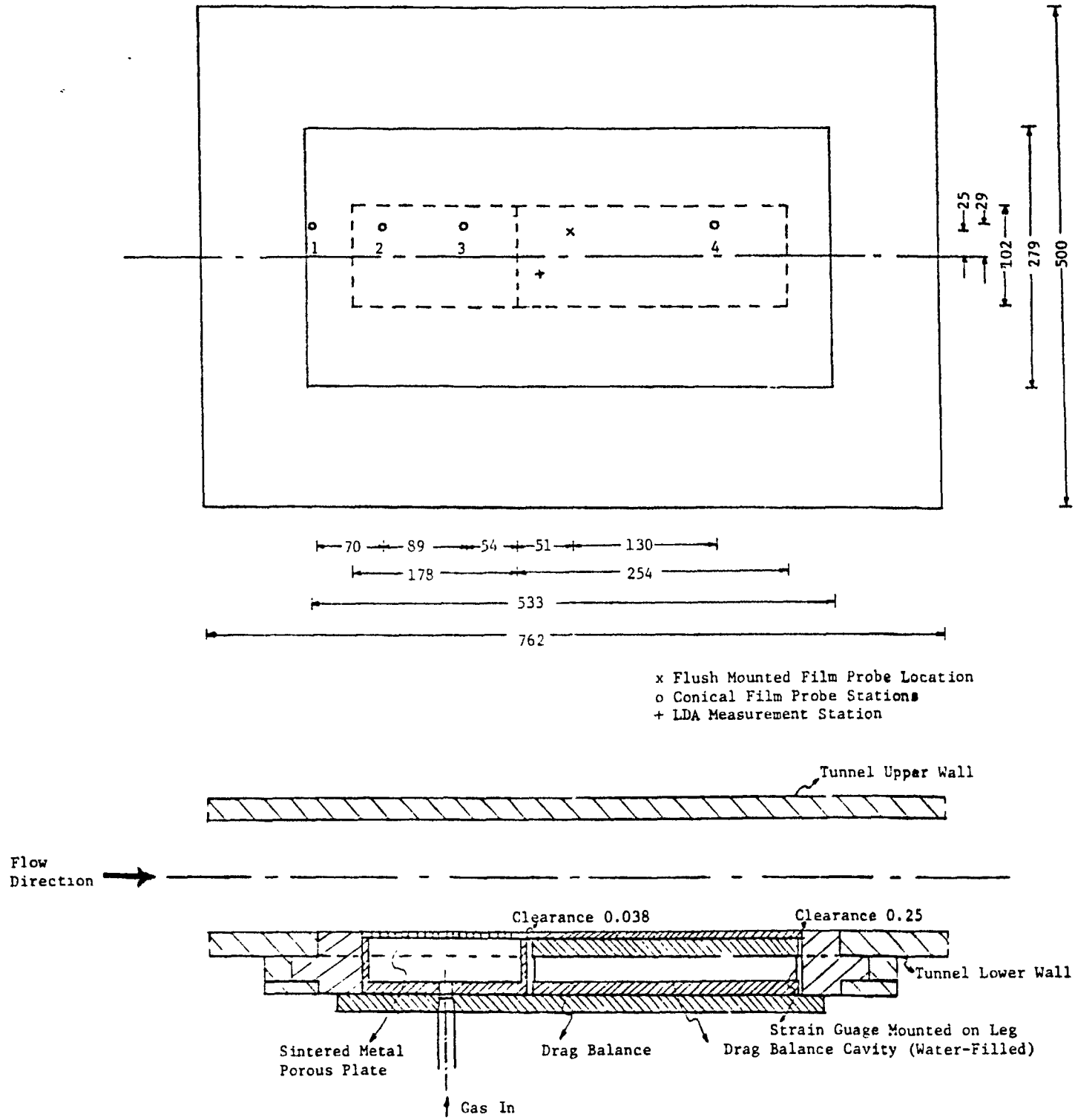

Figure 1: Schematic of Experimental Setup Showing Location of Hot Film and LDA Measurement Stations. (Diagram not to Scale).

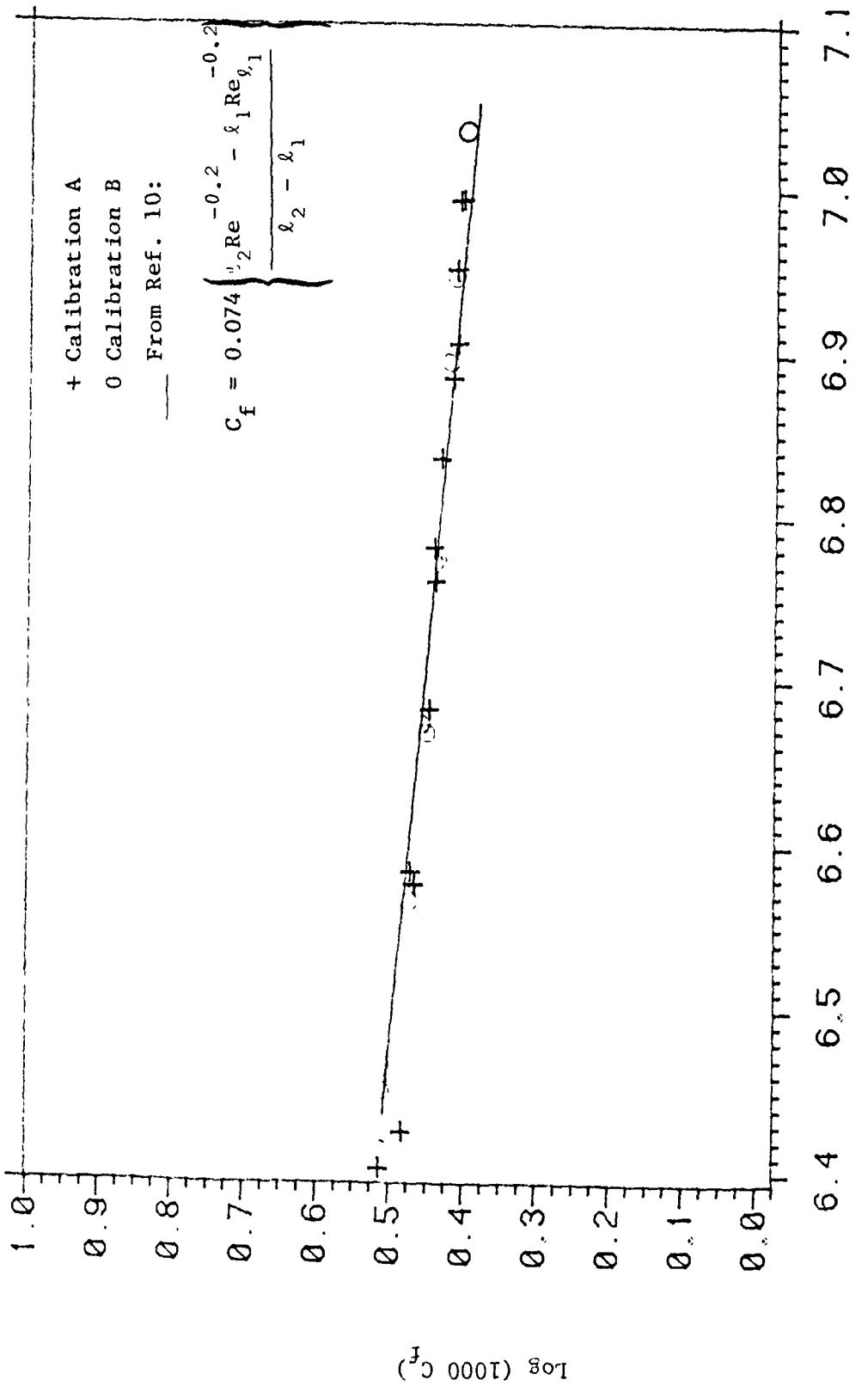

Figure 2: Comparison of Integrated Skin Friction Measurements with Classical Boundary Layer Data. The Symbols ℓ_1 and ℓ_2 Denote Distances to Upstream and Downstream Edge of Drag Balance Respectively from Virtual Origin (356 and 610 mm).

9 March 1983
NKM:SD:CLM:lhm

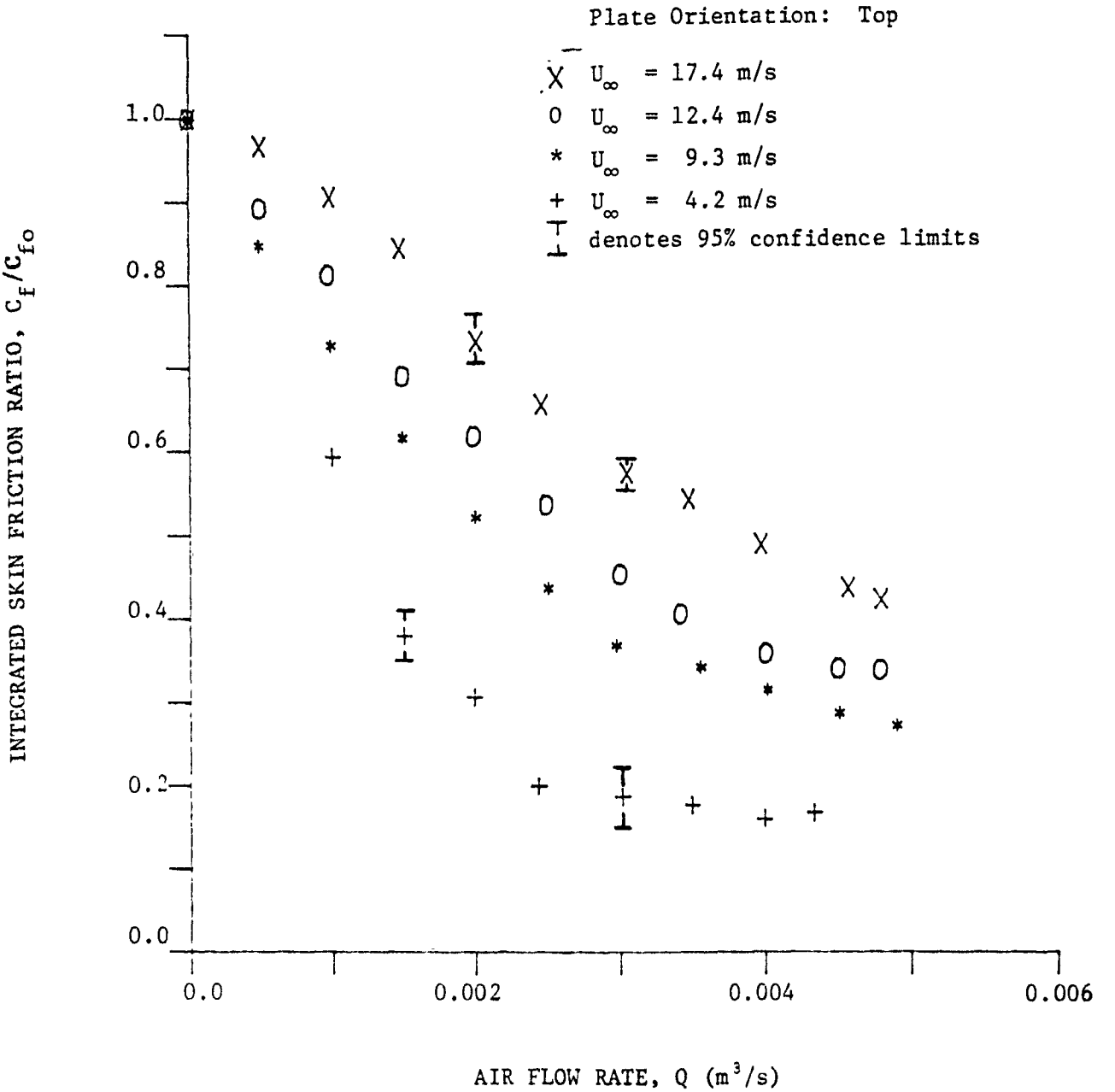

Figure 3: Ratio of Integrated Skin Friction in the Presence of Microbubbles to Skin Friction Without Microbubbles as a Function of Air Flow Rate. Plate Above the Boundary Layer.

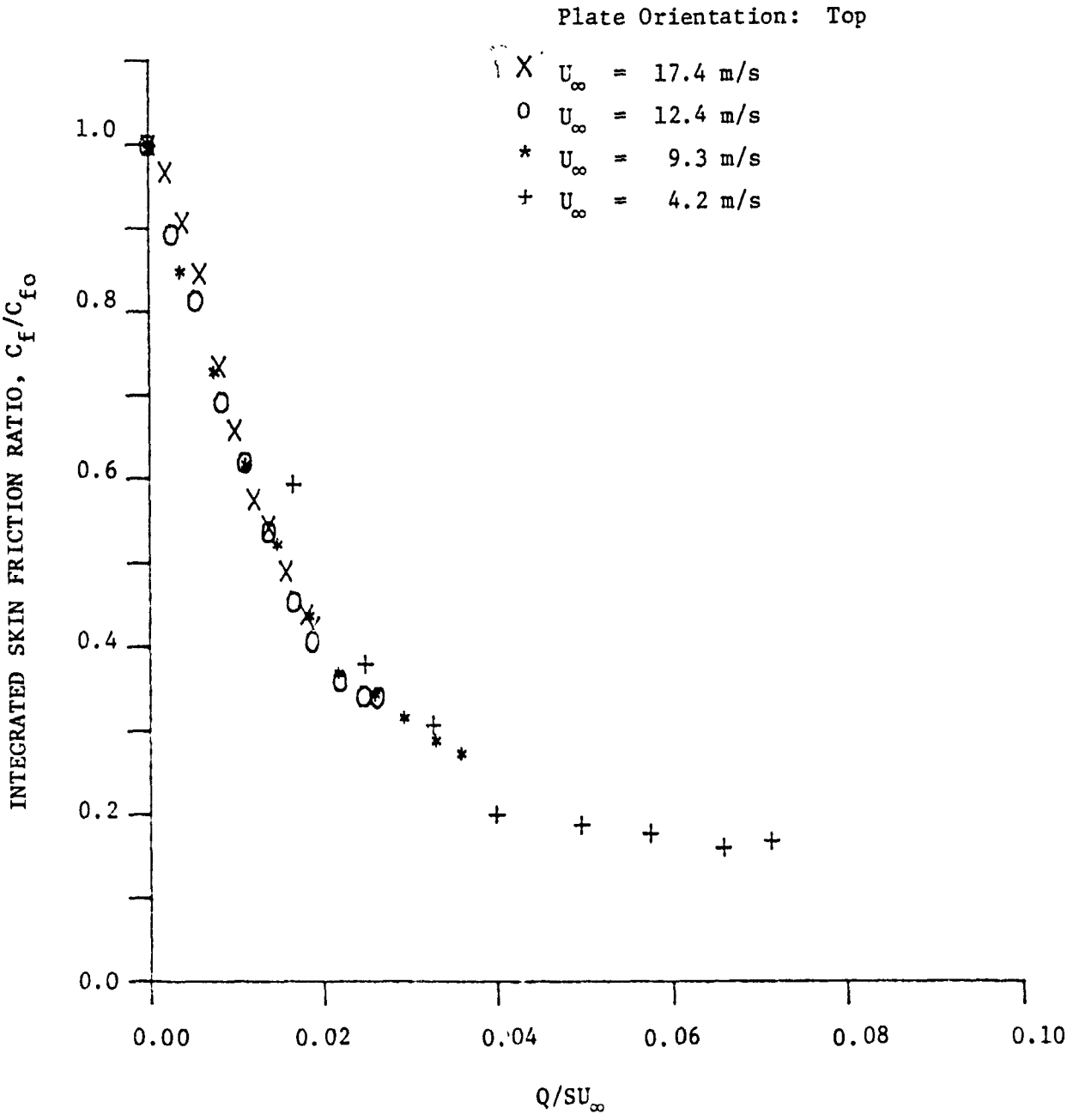

Figure 4: Dimensionless Skin Friction As a Function of Dimensionless Injection Rate. Plate Above the Boundary Layer.

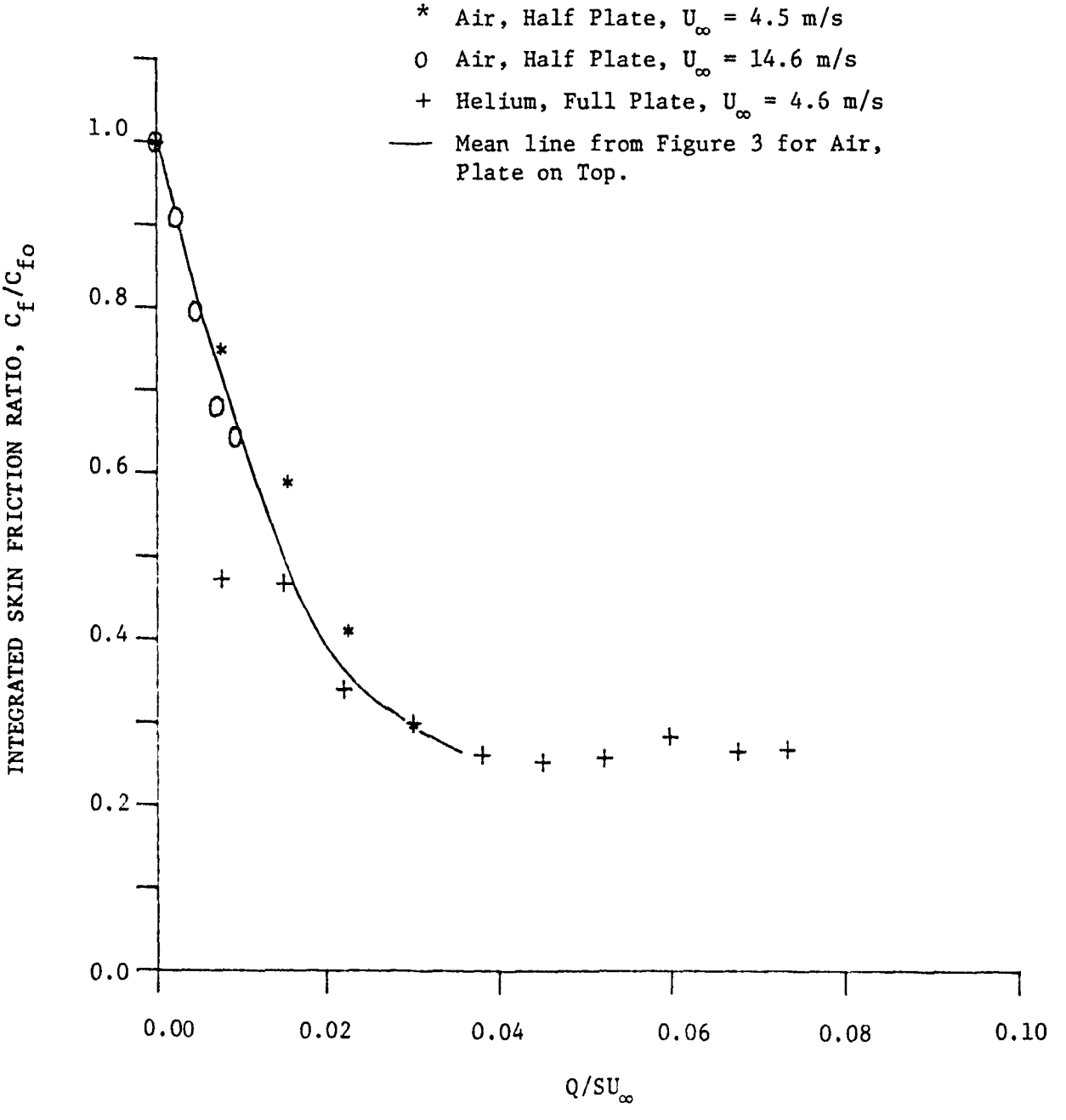

Figure 5: Comparison of the Effects of Using Helium Instead of Air As the Injectant, and of Using Only Half the Porous Plate. Flat Plate Above the Boundary Layer.

9 March 1983
NKM:SD:CLM:lhm

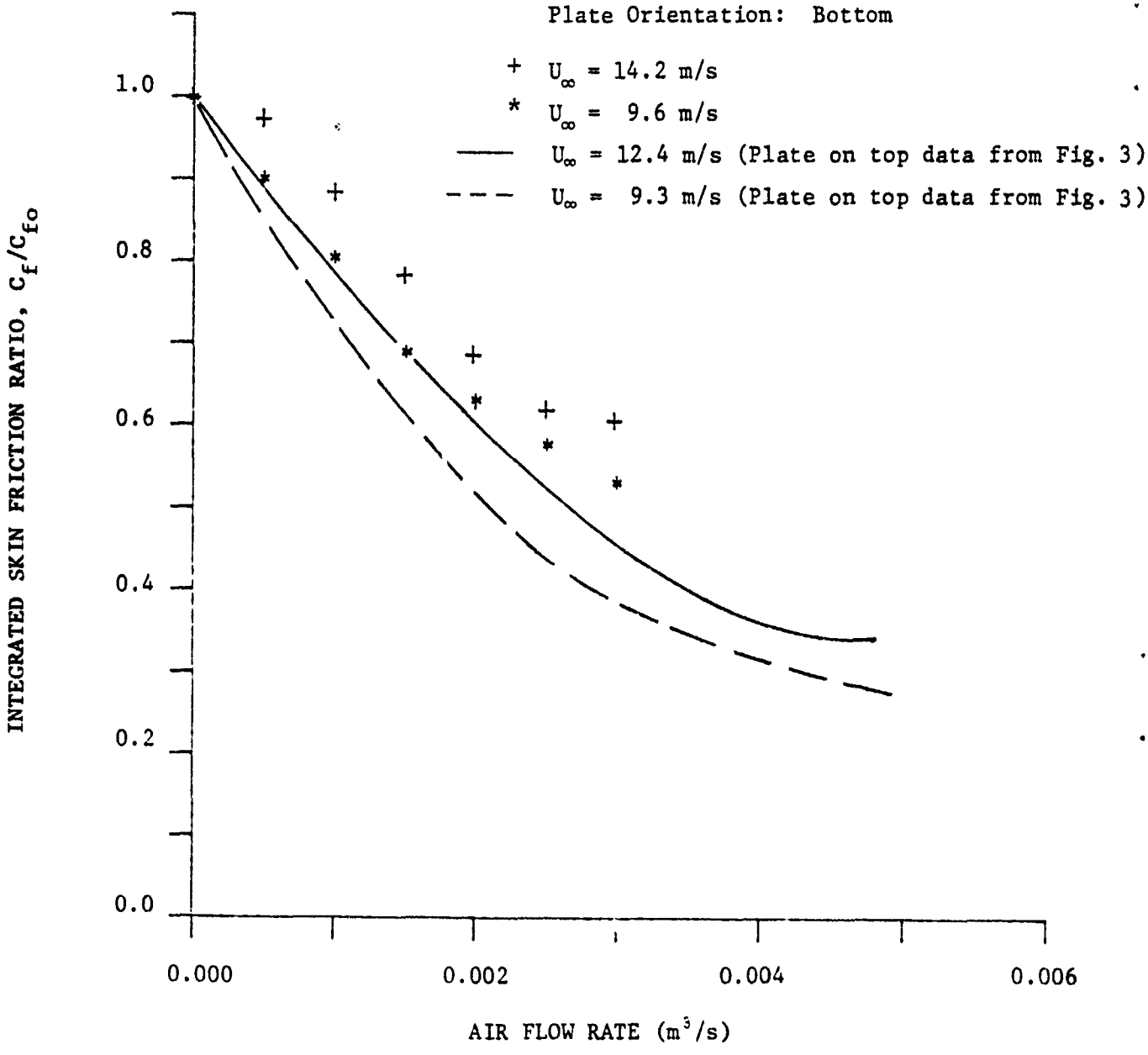

Figure 6: Effects of Buoyancy on Skin Friction Reduction. Comparison of Data Taken With Plate on Top and Plate on Bottom.

9 March 1983
NKM:SD:CLM:lhm

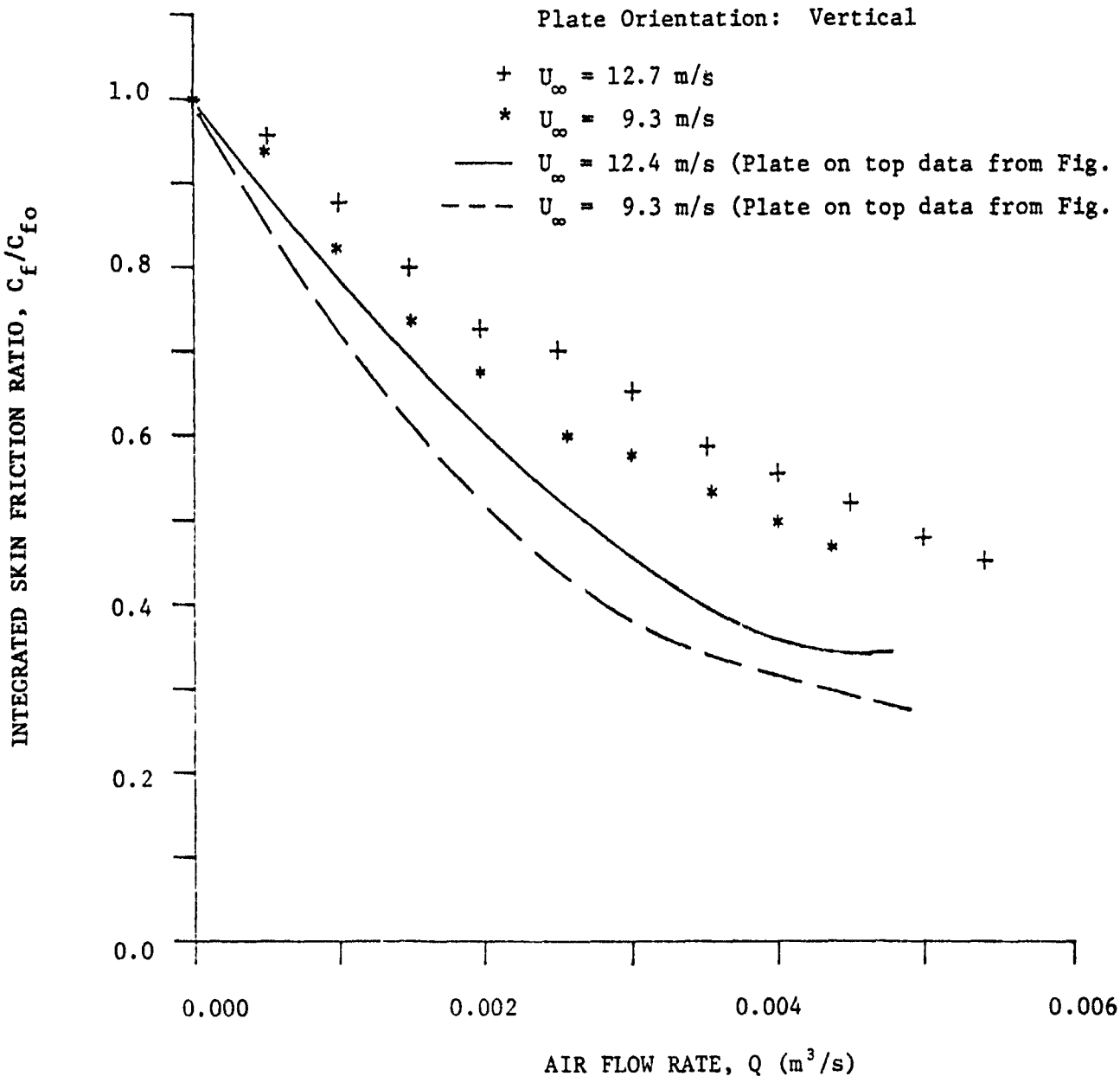

Figure 7: Effects of Buoyancy on Skin Friction Reduction. Comparison of Data Taken with Plate on Top and With Plate Vertical (Along Side of the Boundary Layer).

9 March 1983
NKM:SD:CLM:lhm

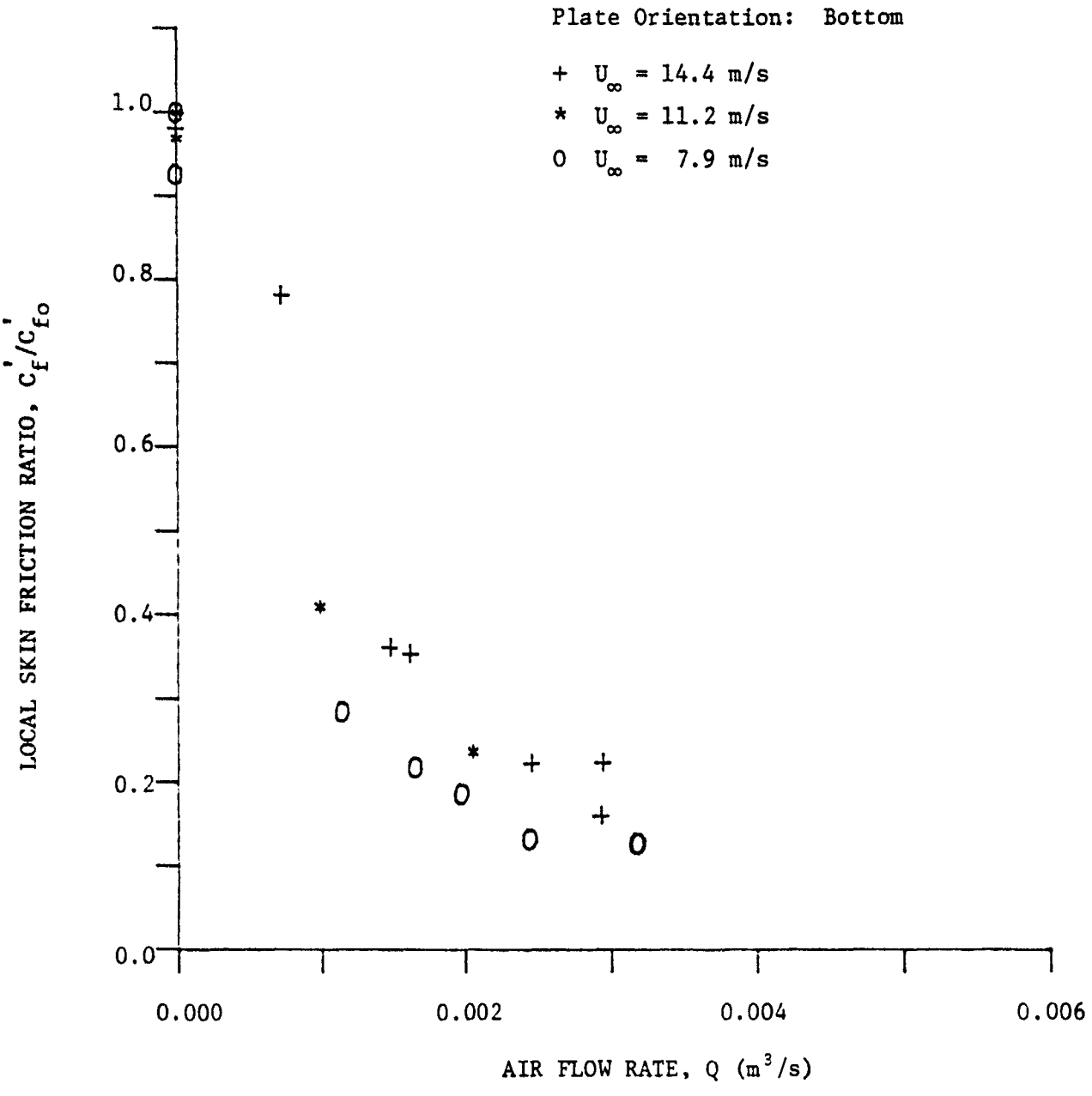

Figure 8. Local Skin Friction as Measured With Surface-Mounted Hot Film. Position of Gage is Noted on Figure 1. Plate on Bottom of Tunnel.

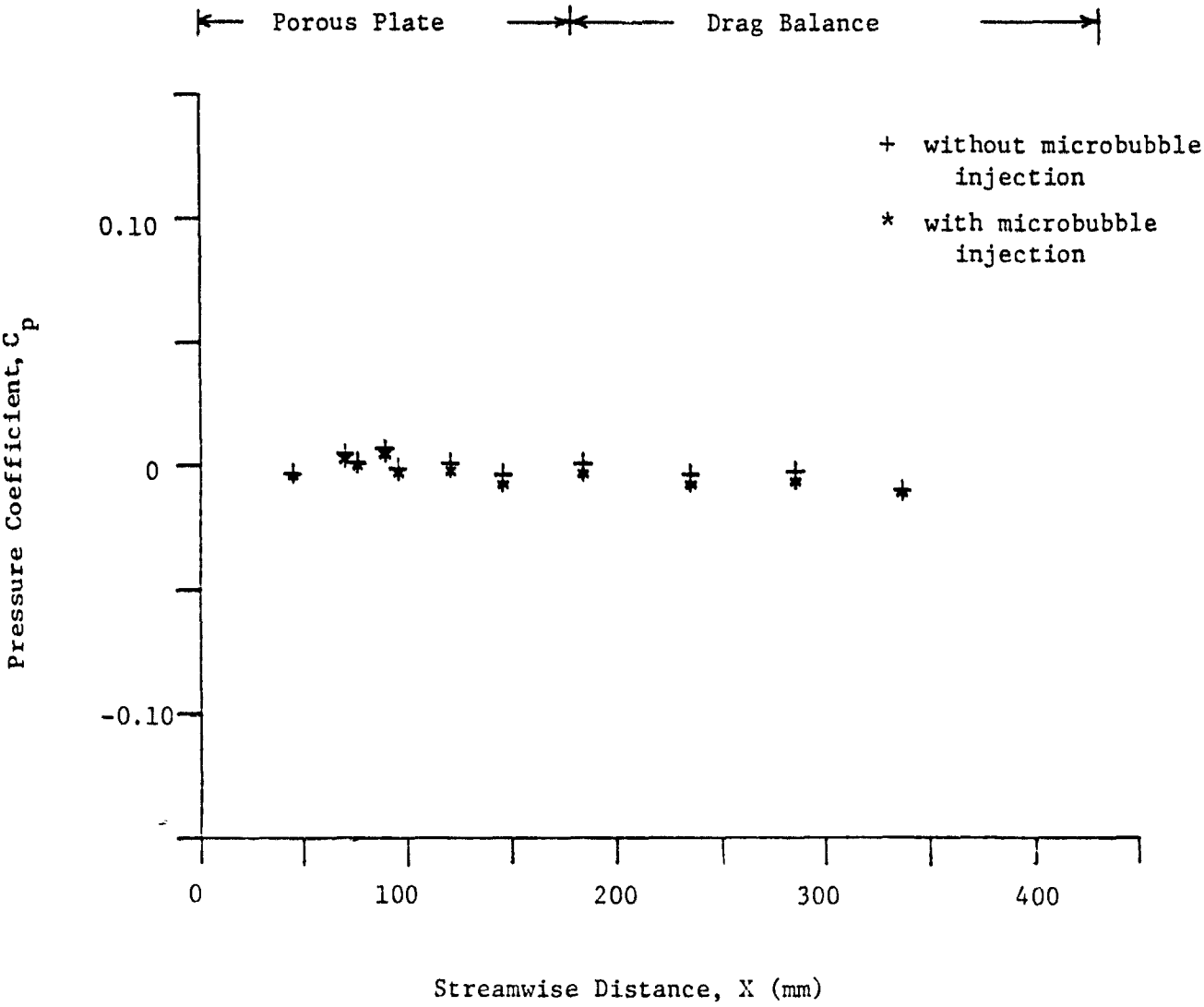

Figure 9: Mapping of Pressure Gradient Along the Test Section.
Distance X is Measured from the Leading Edge of the Porous Plate.

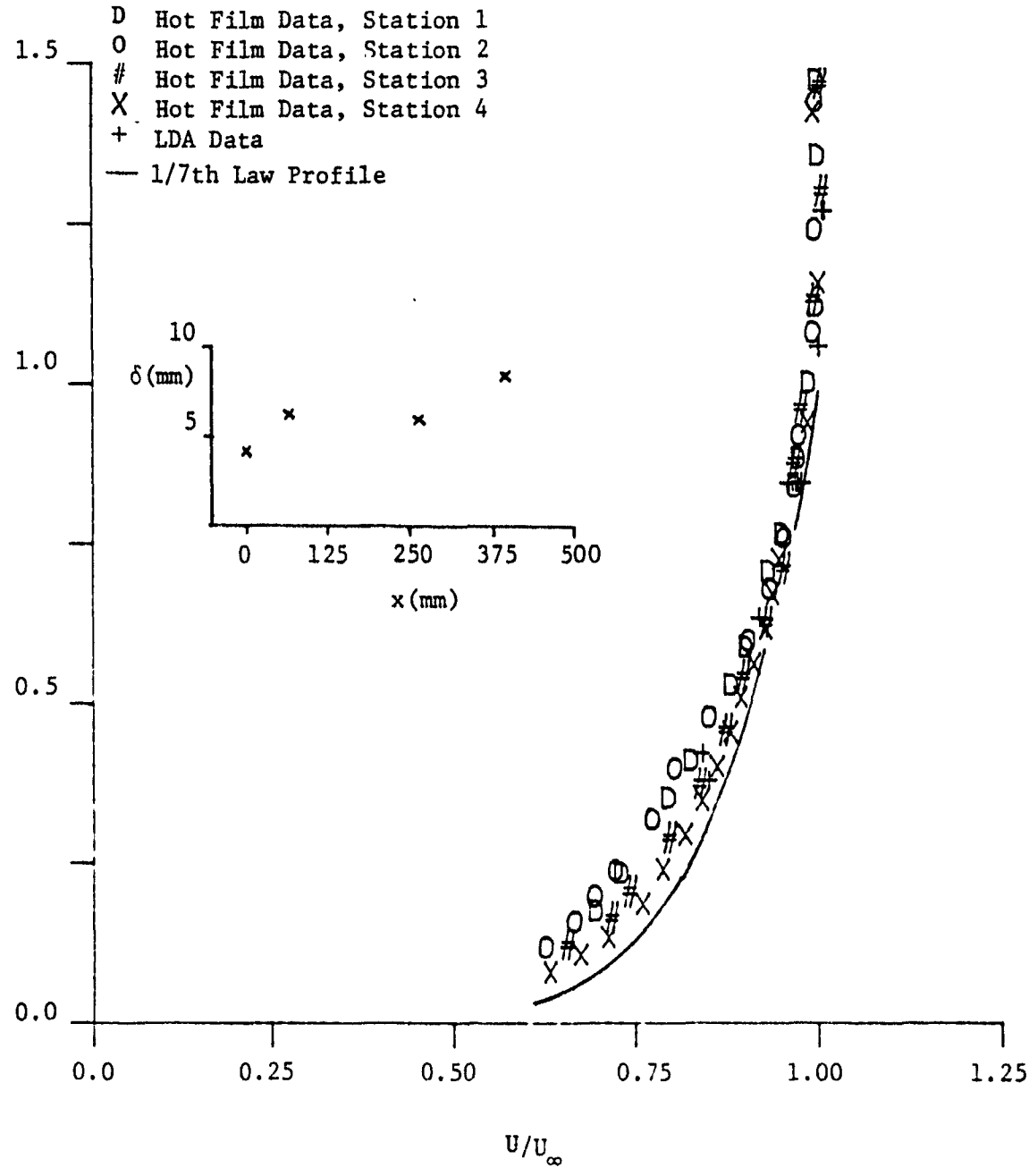

Figure 10: Hot Film and LDA Traverse of Boundary Layer in the Absence of Bubbles. Inset Shows Variation of Boundary Layer Thickness with Streamwise Distance, x. x is Measured From Hot Film Measurement Station 1. Free Stream Velocity: 4.6 m/s for the Hot Film and 7.6 m/s for the LDA Measurements.

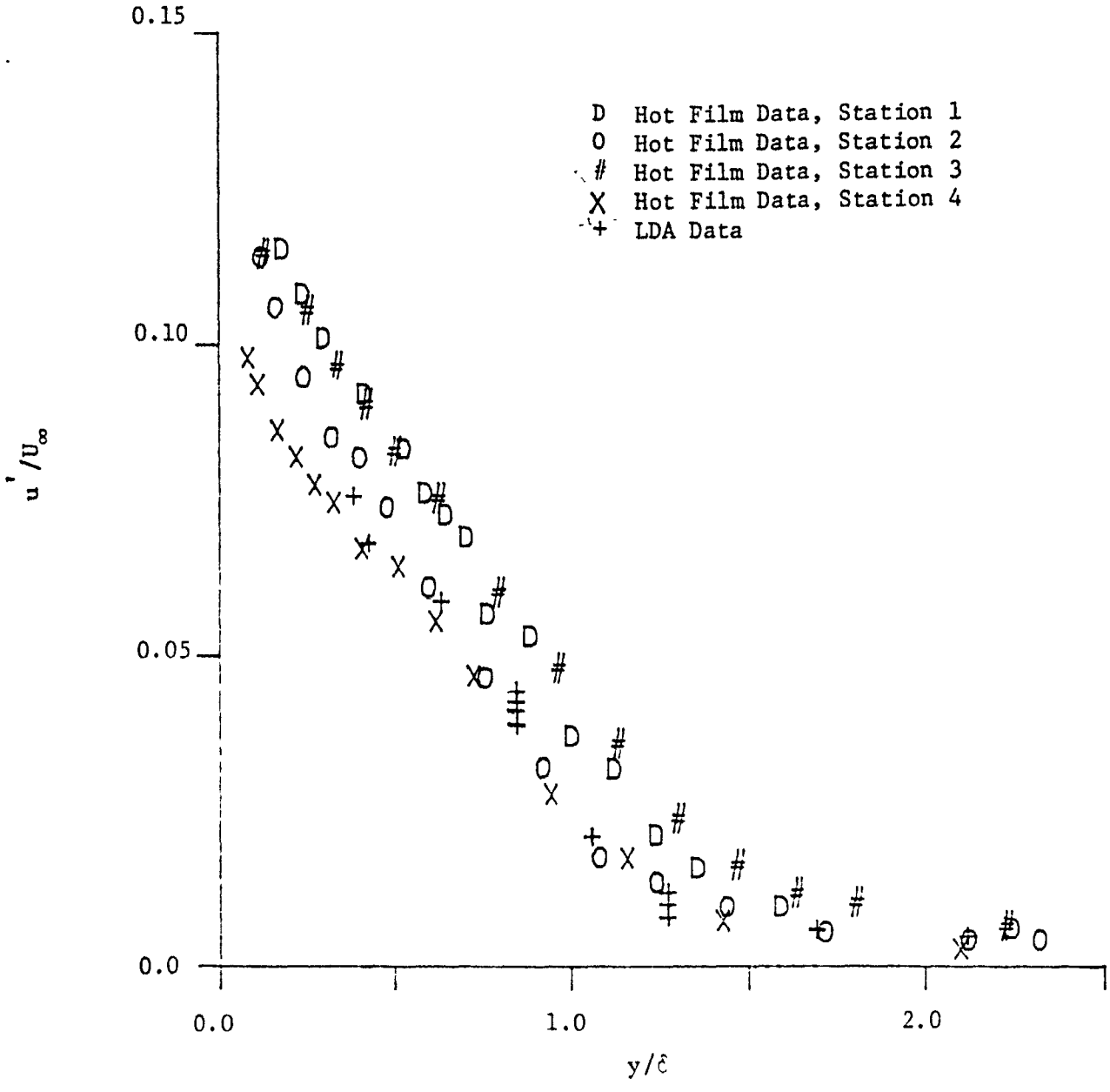

Figure 11: Hot Film and LDA Data of Turbulence Intensity in Outer Part of Boundary Layer. Free Stream Velocity: 4.6 m/s for the Hot Film and 7.6 m/s for the LDA Measurements.

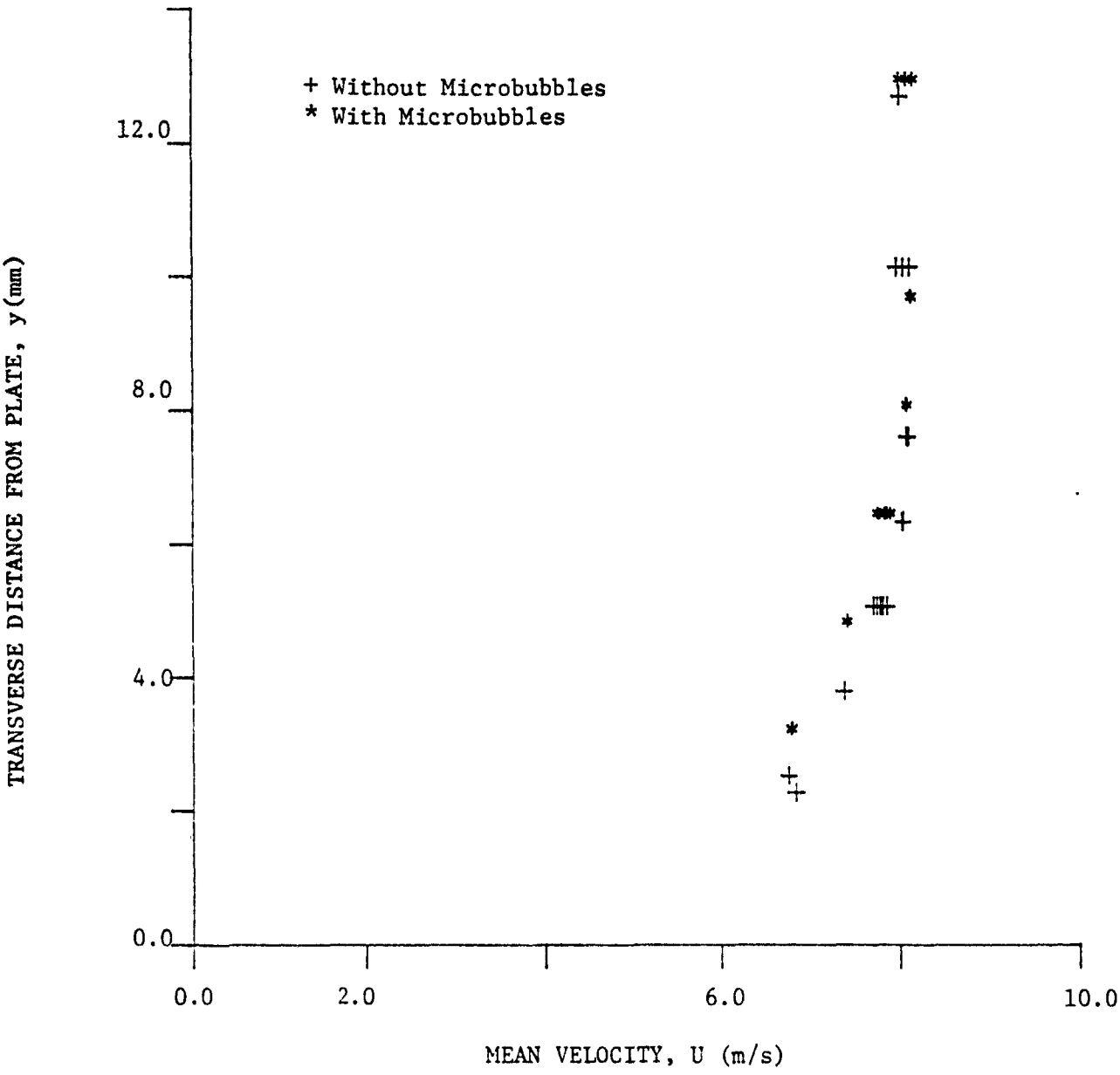

Figure 12: Comparison of Mean Velocity Profiles in Outer Part of Boundary Layer in Presence of Microbubbles and in Absence of Microbubbles.

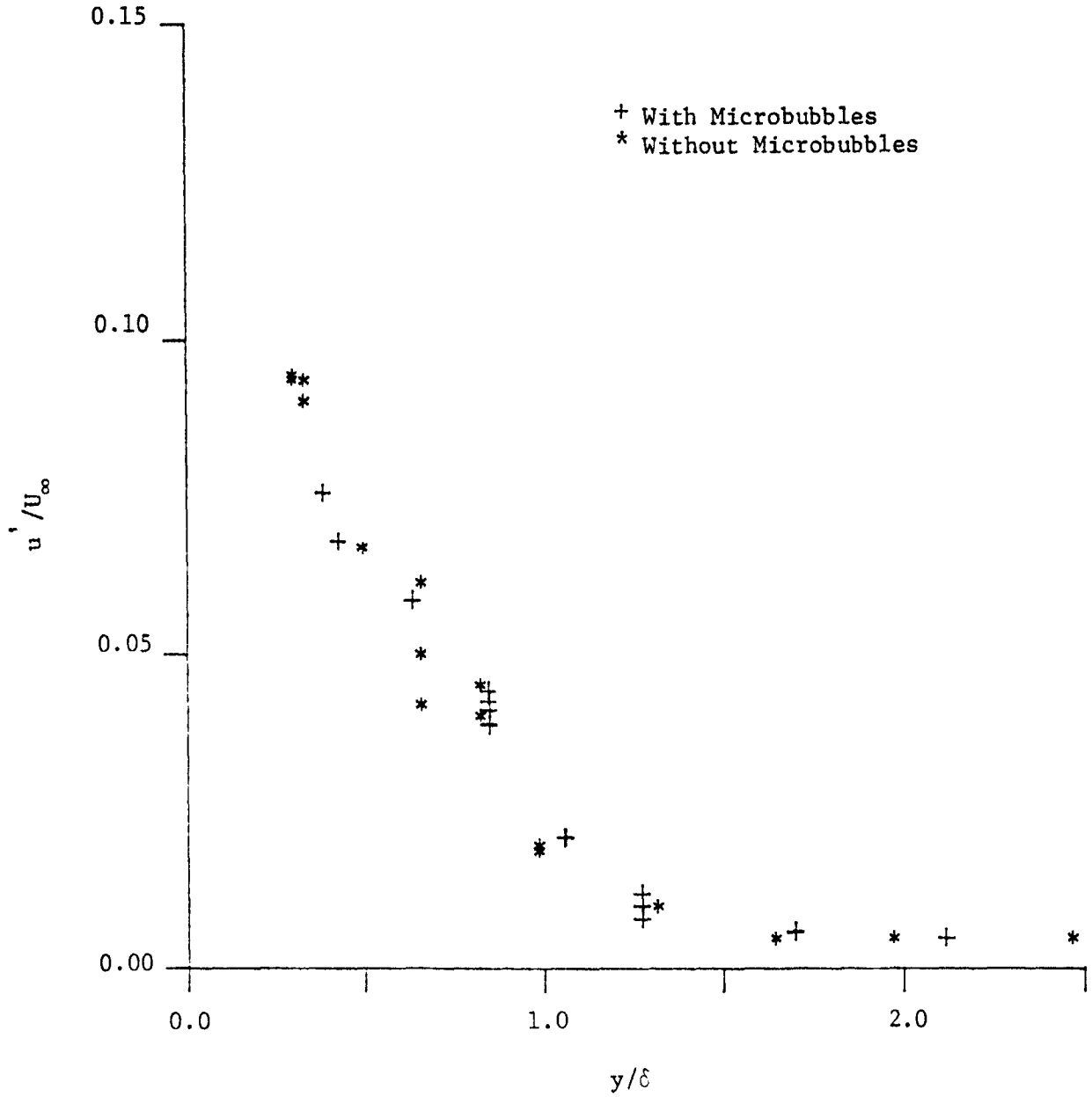

Figure 13: Comparison of Turbulence Intensity in the Outer Part of the Boundary Layer in the Presence of Microbubbles and in the Absence of Microbubbles. Free Stream Velocity Corresponds to Fig. 12.

DISTRIBUTION LIST FOR ARL UNCLASSIFIED TM No. 83-23 by N. K. Madavan, S. Deutsch and C. L. Merkle, dated 9 April 1983.

Commander
Naval Sea Systems Command
Department of the Navy
Washington, DC 20362
Attn: Library
Code NSEA-09G32
(Copies 1 and 2)

Commander
Naval Sea Systems Command
Department of the Navy
Washington, DC 20362
Attn: F. Romano
Code NSEA-63R
(Copy No. 3)

Commander
Naval Sea Systems Command
Department of the Navy
Washington, DC 20362
Attn: T. E. Peirce
Code NSEA-63R31
(Copy No. 4)

Commander
Naval Sea Systems Command
Department of the Navy
Washington, DC 20362
Attn: S. M. Blazek
Code NSEA-55N
(Copy No. 5)

Commander
Naval Sea Systems Command
Department of the Navy
Washington, DC 20362
Attn: A. R. Paladino
Code NSEA-55N
(Copy No. 6)

Commander
Naval Sea Systems Command
Department of the Navy
Washington, DC 20362
Attn: W. D. Marlin
Code NSEA-931E
(COPY No. 7.)

Commander
Naval Sea Systems Command
Department of the Navy
Washington, DC 20362
Attn: E. G. Liszka
Code PMS-406B
(Copy No. 8)

Commanding Officer
Naval Underwater Systems Center
Department of the Navy
Newport, RI 02840
Attn: Library
Code 54
(Copy No. 9)

Commanding Officer
Naval Underwater Systems Center
Department of the Navy
Newport, RI 02840
Attn: T. A. Davis
Code 36314
(Copy No. 10)

Commanding Officer
Naval Underwater Systems Center
Department of the Navy
Newport, RI 02840
Attn: D. Goodrich
Code 3634
(Copy No. 11)

Commanding Officer
Naval Underwater Systems Center
Department of the Navy
Newport, RI 02840
Attn: R. H. Nadolink
Code 3634
(Copy No. 12)

Commanding Officer
Naval Underwater Systems Center
Department of the Navy
Newport, RI 02840
Attn: C. N. Pryor
Code 01
(Copy No. 13)

Commanding Officer
Naval Underwater Systems Center
Department of the Navy
Newport, RI 02840
Attn: C. Hervey
Code 3634
(Copy No. 14)

Officer-in-Charge
David W. Taylor Naval Ship Research
and Development Center
Department of the Navy
Bethesda, MD 20084
Attn: M. M. Sevik
Code 19
(Copy No. 15)

Officer-in-Charge
David W. Taylor Naval Ship Research
and Development Center
Department of the Navy
Bethesda, MD 20084
Attn: J. H. McCarthy
Code 154
(Copy No. 16)

Officer-in-Charge
David W. Taylor Naval Ship Research
and Development Center
Department of the Navy
Bethesda, MD 20084
Attn: T. T. Huang
Code 1552
(Copy No. 17)

Officer-in-Charge
David W. Taylor Naval Ship Research
and Development Center
Department of the Navy
Bethesda, MD 20084
Attn: J. Shen
Code 194
(Copy No. 18)

Commander
Naval Surface Weapons Center
Department of the Navy
Silver Spring, MD 20910
Attn: G. C. Guanaurd

Office of Naval Research
800 North Quincy Street
Department of the Navy
Arlington, VA 22217
Attn: R. Whitehead
Code 432
(Copy No. 20)

Office of Naval Research
800 North Quincy Street
Department of the Navy
Arlington, VA 22217
Attn: M. M. Reischman
Code 432F
(Copy No. 21)

National Bureau of Standards
Aerodynamics Section
Washington, DC 20234
Attn: P. S. Klebanoff
(Copy No. 22)

National Bureau of Standards
Aerodynamics Section
Washington, DC 20234
Attn: J. M. McMichael
(Copy No. 23)

Naval Research Laboratory
Department of the Navy
Washington, DC 20390
Attn: R. J. Hansen
(Copy No. 24)

Rand Corporation
1700 Main Street
Santa Monica, CA 90406
Attn: R. King
(Copy No. 25)

Rand Corporation
1700 Main Street
Santa Monica, CA 90406
Attn: J. Aroesty
(Copy No. 26)

Rand Corporation
1700 Main Street
Santa Monica, CA 90406
Attn: C. Gazley
(Copy No. 27)

Rand Corporation
1700 Main Street
Santa Monica, CA 90406
Attn: A. R. Wazzan
(Copy No. 28)

Dynamics Technology, Inc.
22939 Hawthorne Blvd.
Suite 200
Torrance, CA 90505
Attn: W. W. Haigh
(Copy No. 29)

Dynamics Technology, Inc.
22939 Hawthorne Blvd.
Suite 200
Torrance, CA 90505
Attn: G. L. Donohue
(Copy No. 30)

Mr. W. M. Phillips
Chairman
Department of Mechanical Engineering
Purdue University
Lafayette, IN 47907
(Copy No. 31)

Mr. Robert F. Mons
Westinghouse Electric Corporation
Post Office Box 1458
Annapolis, MD 21404
(Copy No. 32)

Prof. J. L. Lumley
Sibley School of Engineering
Cornell University
Ithaca, NY 14850
(Copy No. 33)

Applied Research Laboratory
The Pennsylvania State University
Post Office Box 30
State College, PA 16801
Attn: B. R. Parkin
(Copy No. 34)

Applied Research Laboratory
The Pennsylvania State University
Post Office Box 30
State College, PA 16801
Attn: R. E. Henderson
(Copy No. 35)

Applied Research Laboratory
The Pennsylvania State University
Post Office Box 30
State College, PA 16801
Attn: S. Deutsch
(Copy No. 36)

Applied Research Laboratory
The Pennsylvania State University
Post Office Box 30
State College, PA 16801
Attn: G. B. Gurney
(Copy No. 37)

Applied Research Laboratory
The Pennsylvania State University
Post Office Box 30
State College, PA 16801
Attn: Water Tunnel Files
(Copy No. 38)